Surface Science 606 (2012) 1618–1622

Contents lists available at SciVerse ScienceDirect

Surface Science

journal homepage: www.elsevier.com/locate/susc

Measurement of the sputter yield after mild ion erosion of a pristine Cu(001) surface

Georgiana Stoian [1], Raoul van Gastel, Herbert Wormeester *, Bene Poelsema

Physics of Interfaces and Nanomaterials, MESA + Institute for Nanotechnology, University of Twente, P.O. Box 217 Enschede, The Netherlands

ARTICLE INFO

Article history:
Received 2 February 2012
Accepted 29 June 2012
Available online 16 July 2012

Keywords:
Sputter yield
Ion beam induced defects
STM

ABSTRACT

Using the STM technique we have determined the sputter yield on a pristine Cu(001) surface after mild (fluence less than 0.044 ions per surface atom) bombardment of the pristine surface with 800 eV Ar^+ions at normal incidence. The experiments have been performed at substrate temperatures ranging from 200 to 350 K. Making use of the positional correlation of adatoms and surface vacancies, at 200 K and 325 K, we concluded that about 1/3 of the surface adatoms originate from interstitials arriving at the surface and they give a direct indication of the buried bulk vacancies. A careful analysis of the different areas for surface vacancies and adatom then allowed a quantitative evaluation of the sputter yield at 1.2 Cu atoms per 800 eV Ar^+ ion.

1. Introduction

Noble gas ion beam erosion, also referred to as ion sputtering, is nowadays a versatile process in surface science. Its applications range from surface preparation [1] and surface/bulk analysis [2] to fabrication of well-ordered nanostructures with specific properties [3–6]. Energetic ions impinging on a solid target eject target atoms, i.e. they cause sputtering. A quantitative measure for the effect of ion sputtering is the *sputter yield*, which is the average number of atoms ejected from the solid per incident ion.

The classical method to experimentally measure the value of the sputter yield is to measure the weight loss of a target subjected to a known ion fluence [7]. The disadvantage of this technique is that the sample has to be taken out from vacuum to be weighed. Despite of this drawback, the weight loss method has been employed to determine the sputter yield after extended bombardment for a large number of different ion-target combinations [8]. In-situ measurement of the sputter yield was later performed with the help of a quartz oscillator crystal, which acted as a support for the target material [9]. In-situ measurements of sputter yields of pristine crystal surfaces have been reported for Pt(111), making use of Thermal Energy Atom Scattering (TEAS) [10,11]. However, this approach is restricted to relatively high sample temperatures.

In the late eighties the Scanning Tunneling Microscope (STM), a new technique at that time, has proven to be a powerful tool to address the question of ion-solid interaction. Since then, a great number of studies have employed STM to investigate ion erosion on a broad variety of metals [12–14]. Most of these studies are concerned with morphological changes after ion bombardment and to a much smaller extent with the determination of the sputter yield. The advantage of the STM technique over the previously used weight loss method is its ability to tackle the sputter yield after mild erosion. In the nineties, Michely and Teichert performed a systematic STM investigation of the energy dependence of the sputter yield of the Pt(111) surface after mild erosion with various noble gas ions [16]. In addition, STM has demonstrated its ability to resolve single ion impacts on Ag(001) [13], Pt(111) [14] and has even been able to distinguish differences in the sputter yield at steps and terraces after grazing incidence ion beam bombardment on Pt (111) [12].

Parallel to the experimental developments, understanding of the sputtering process on the atomic level has been achieved through computer simulations. Molecular Dynamics simulations were employed by Gades and Urbassek [15] to estimate the sputter yield of the Pt(111) surface when exposed to rare gas ion bombardment at ion energies between 100 and 3000 eV. The calculated sputter yield was consistent with previously reported experimental results [16]. The energy dependence of the sputter yield of Cu(001), sputtered with 10–2500 eV Ar^+ ions, was calculated by Promokov et al. by means of Molecular Dynamics simulations [17]. These authors obtained good agreement with the experimental weight loss data of Snouse [18] and Southern [19] finding a sputter yield of 2.3 atoms/ion.

In this paper we perform a STM investigation of the sputter yield after normal incidence Ar^+ ion beam erosion of a pristine Cu(001) surface. Experimental investigations of the sputter yield for this system date back to the sixties and have been made using the weight loss method. Our present STM investigation is triggered by the importance of the sputter yield in the formation of ion beam induced nanostructures. An experimental value of the sputter yield is not known for the *pristine* Cu(001) substrate. Such a number is required for the fabrication of nanostructures or patterning of single crystal surfaces with an ion beam. STM in principle can establish the value of the sputter yield

* Corresponding author. Tel.: +31 53 489 3148/3147; fax: +31 53 489 1101.
E-mail addresses: f.g.stoian@gmail.com (G. Stoian), r.vangastel@utwente.nl (R. van Gastel), h.wormeester@utwente.nl (H. Wormeester), b.poelsema@utwente.nl (B. Poelsema).
[1] Present address: Department of Radiation Oncology, The University Medical Center Groningen, The Netherlands.

0039-6028/$ – see front matter © 2012 Elsevier B.V. All rights reserved.
doi:10.1016/j.susc.2012.06.013

during the initial stages of ion bombardment. Moreover, we demonstrate here that it allows the sputter yield to be measured without the need for any additional thermal treatment after sputtering. The use of STM for this purpose can however be cumbersome because of potentially large tip convolution effects with adatoms and vacancies. We present a recipe that systematically addresses errors introduced by this effect.

2. Experimental procedure

The experiments were carried out in an Ultra High Vacuum (UHV) chamber with a base pressure lower than $2\cdot10^{-10}$ mbar. The cleaning procedure of the Cu(001) sample was accomplished by 800 eV Ar^+ ion bombardment at room temperature followed by 10 min annealing at 773 K. The ion fluence during the cleaning procedure was $4\cdot10^{16}$ ions$\cdot$cm^{-2}. For the ion bombardment experiments, the clean and well-annealed Cu(001) sample was exposed to a flux of $8.76\cdot10^{11}$ ions$\cdot$cm$^{-2}\cdot$s^{-1} and an ion dose of $6.75\cdot10^{13}$ ions$\cdot$cm^{-2}, which corresponds to 0.044 monolayer equivalent (MLE). For the Cu(001) surface, 1.00 MLE is equal to an ion dose of $1.53\cdot10^{15}$ ions$\cdot$cm^{-2}. The ion flux was calibrated using a Faraday cup with an aperture diameter of 2 mm placed at the sample position in front of the ion gun. We have deliberately defocused the ion beam to ensure that the ion flux is homogeneous over the entire Cu(001) surface area. The experiments were performed at variable substrate temperatures from 200 K up to 350 K, at increments of 25 K. As soon as the sputter experiment ended, the ion gun was switched off and the freshly eroded Cu(001) substrate was rapidly cooled to 110 K to prevent or at least minimize subsequent surface reorganization. Thereafter, the surface topography was imaged with a Scanning Tunneling Microscope (STM). The STM images are recorded in constant current mode at 0.44 V and 0.4 nA, if not otherwise specified. Experiments performed at temperatures greater than 350 K did not yield accurate data because of abundant annealing and recombination of the produced defects at steps.

To accurately determine the correct threshold position for image analysis, a planar image background was subtracted and a histogram of the surface heights was made. The peak positions that were visible in the histogram for the substrate, adatom and vacancy levels were determined by fitting a Gaussian profile to each. The threshold to discriminate between the three possible identifications of a pixel in the STM images, was then determined by taking the median value between the respective peaks.

3. Results

The surface topographies measured with the STM after ion erosion with an ion fluence of 0.044 MLE at substrate temperatures in the range of 200 K–350 K, are shown in Fig. 1(a)–(g). The temperature dependent morphology in Fig. 1 can be rationalized in terms of competition between the erosive effect of the ion beam and the smoothening effect of thermal diffusion.

At the lowest substrate temperatures used in our experiments, surface diffusion on Cu(001) is very limited and the morphology is mostly governed by the erosive effect of the impinging ions which leads to simultaneous creation of adatom and vacancy clusters. In Fig. 1 the monatomically high adatom and vacancy clusters are represented by bright and dark areas, respectively. Although surface diffusion is negligible below 230 K, the ion impact causes a local enhancement in surface mobility around the impact point [4]. The ion impact driven surface diffusion enables the point defects created in the single ion impacts and those originating from neighboring ion impacts to partly coalesce. The result is a high density of small, irregularly shaped adatom and vacancy clusters (see Fig. 1(a)–(b)).

At intermediate substrate temperatures, surface diffusion is activated and larger adatom and vacancy islands are formed (Fig. 1(c)–(d)). A decrease of the cluster density is observed accompanied by an increase of the average cluster area.

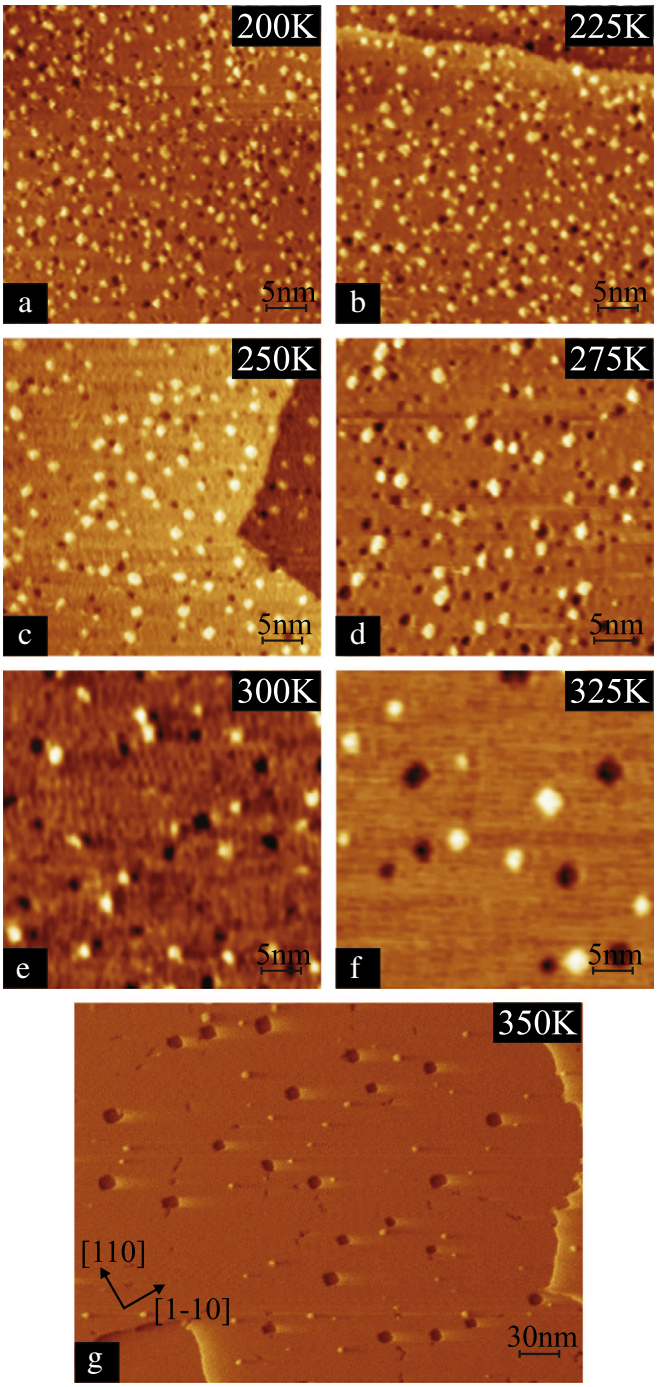

Fig. 1. STM topographies of the Cu(001) surface after bombardment with 800 eV Ar^+ ions, at normal incidence with a ion fluence of 0.044 MLE, for various substrate temperatures, from 200 K up to 350 K. Image sizes: (a)–(f) 40×40 nm^2 and (g) 350×250 nm^2, tunneling current 0.5 nA and tunneling voltage 0.4 V.

At high temperatures (Fig. 1(e)–(g)) surface diffusion is very effective. The surface morphology exhibits low densities of large adatom and vacancy islands. The efficient diffusion of atoms along steps allows the adatom and vacancy islands to assume their equilibrium shape: square with rounded corners. The steps of the islands follow the high symmetry [110] and [$\bar{1}$10] crystallographic directions of the Cu(001) surface. At 350 K most of the adatoms that are formed after an ion impact annihilate with the vacancy islands and the surviving vacancies coalesce into larger clusters. It is worthwhile to

note the large terrace area in Fig. 1(g). Such large terraces are necessary to properly quantify the defects caused by ion bombardment at high temperatures. The steps between terraces act as sinks for diffusive species present on the surface. Because of this, an unknown fraction of the defects created by ion impacts in the immediate vicinity of a step cannot be observed.

4. Analysis and discussion

The impact between the energetic argon ions and the Cu(001) surface leads to collision cascades in the top layers of the target. During the collision cascades some atoms acquire sufficient energy to overcome the surface binding energy and permanently leave the surface. As the collision cascades end, various types of defects remain at the impact sites. Defects are found both at the surface (surface vacancies and adatoms) as well as in the bulk, bulk vacancies and interstitials, of the copper target. The latter appear naturally when a bulk atom is kicked out of its lattice position and is promoted to become an interstitial. Such vacancy — interstitial defect pairs are known as Frenkel pairs. As discussed further below, in all subsequent cases the interstitials will arrive at the surface to finally form an adatom (bulk-) vacancy, i.e. Schottky-, pair. For higher fluences, the trapped ions (or better neutrals) may form clusters and sub-surface vacancy clusters.

A quantitative description of the sputter yield is expressed in terms of the defects left behind by the ion-substrate collision. The integrated areas of vacancy clusters and adatom clusters in Fig. 1 provide two out of the three parameters needed to determine the sputter yield as defined in Eq. (1):

$$Y = \frac{\theta^{sv} + \theta^{bv} - \theta^{ad}}{\theta^{ion}} \tag{1}$$

where θ indicates the relative coverages of surface vacancies (θ^{sv}), bulk vacancies (θ^{bv}), and adatoms (θ^{ad}). θ^{ion} is the ion dose used in our experiments, equal to 0.044 MLE. The interstitials that are formed in the sputter events are already mobile at 45 K in the copper substrate [20]. This implies that at the substrate temperatures used the interstitials will either have annihilated with nearby bulk vacancies or have segregated to the surface, with a subsequent interaction with surface defects (through annihilation with surface vacancies or transformation into adatoms) prior to the start of the STM measurements. These annihilation events reduce the number interstitials to zero and changes the individual contributions in the numerator of Eq. (1), but does not alter the balance between vacancies and adatoms. The effect of interstitials can therefore be neglected in the sputter yield as defined in Eq. (1). Bulk vacancies have a more complicated annealing behavior and they have a tendency to become lodged in the subsurface region, where they have been created. For obvious reasons, these bulk defects are not detectable by STM. At relatively low substrate temperatures (well) below 25% of the melting temperature, bulk vacancies are immobile and thus remain hidden at their native, near surface positions [21]. Therefore, from STM images we can only infer the *apparent sputter yield* Y^*, defined as:

$$Y^* = \frac{\theta^{sv} - \theta^{ad}}{\theta^{ion}} \tag{2}$$

As a first approximation we can assume the sputter yield Y to be equal to the apparent sputter yield Y^*. Fig. 2 shows the temperature dependence of the adatom and vacancy coverage. The apparent sputter yield inferred from Eq. (2) is plotted in the inset of Fig. 2.

At low substrate temperatures, the adatom coverage far exceeds the coverage of surface vacancies. This implies that the apparent sputter yield has a negative value, as shown in the inset in Fig. 2. Whereas a negative value can be obtained for the *apparent* sputter yield under certain conditions, obviously a negative sputter yield is physically not realistic. Moreover, a sizeable temperature dependence of the sputter yield is not expected [22,23] since the bulk vacancies do not play a role in this temperature regime, as discussed above. Still working with the assumption $Y = Y^*$, this seemingly unphysical behavior of the sputter yield is caused by the strong systematic convolution effects inherent to the STM imaging technique and by the hidden bulk vacancies that are formed upon ion impact. These factors contribute to a considerable underestimation of the surface area covered by vacancy clusters, which in turn diminishes the value of the apparent sputter yield. In the high temperature regime, our measurement of the apparent sputter yield is improved because the interfering factors are mitigated. At elevated temperatures the previously trapped bulk vacancies may segregate toward the surface were they join pre-existing surface vacancies or are annihilated. However, as stated above, a contribution of bulk diffusion in the temperature regime under consideration here can be neglected [21]. In addition, adatom and surface vacancy clusters might coalesce to form larger ones. In doing so, they reduce their boundary length, which leads to reduced convolution effects. Taking into account the above mentioned factors, at high temperatures the apparent sputter yield Y^* should be similar to the absolute sputter yield Y, except for the remaining near surface bulk vacancies.

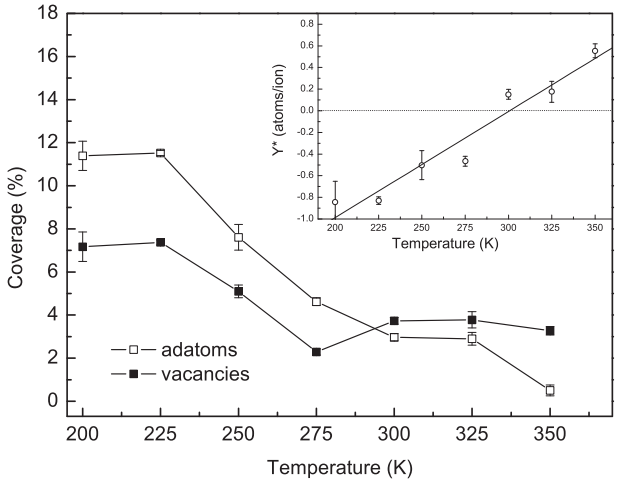

Fig. 2. Surface vacancy and adatom coverages versus substrate temperature after 800 eV Ar^+ ion bombardment of Cu(001) with a fluence of 0.044 MLE. The inset shows the apparent sputter yield as defined by Eq. (2). The solid line in the inset guides the eye for the temperature dependence of the apparent sputter yield.

Uncertainties in the coverage measurement of monatomically high adatom clusters, respectively, monatomically deep vacancy clusters obviously provide a problem for the accurate determination of the sputter yield from STM measurements. However, we can estimate the magnitude of the convolution features and their consequence for the present analysis. Besides our assumption of low diffusivity of bulk vacancies [21], we also assume that in the entire temperature range considered here, the interstitials will have either moved toward the surface or have annihilated previously formed bulk vacancies while being on their journey toward the surface [20]. Moreover, we assume that the sputter yield does not depend on the substrate temperature, since no evidence has been reported for temperature dependence over a wide temperature range. With this set of physically acceptable assumptions we now address the convolution issue. The uncertainty in the exact position of an adatom cluster or a vacancy cluster's circumference is given by ΔN^{ad} and ΔN^{vac}, respectively, as sketched in Fig. 3. The real area of an adatom cluster with an apparent area of N^{ad} is then approximately $[(N^{ad})^2 - 4N^{ad}\Delta N^{ad} + 4(\Delta N^{ad})^2]$. A similar argument holds for the real size of a vacancy cluster with an apparent size of N^{vac} which is then approximated by $[(N^{vac})^2 + 4N^{vac}\Delta N^{vac} + 4(\Delta N^{vac})^2]$.

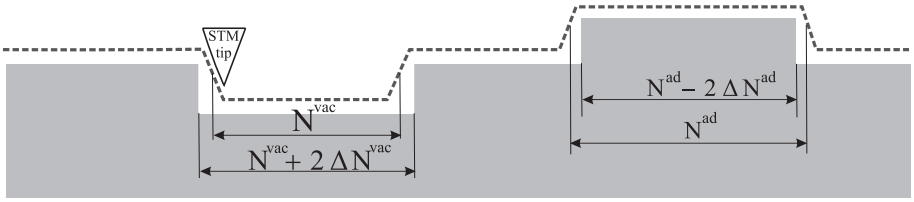

Fig. 3. Schematic representation of the convolution effects induced by the STM tip for a vacancy (left) and adatom island (right). See text for discussion.

Obviously, the magnitude of convolution effect depends on the exact shape of the STM-tip, which can in fact change during the experiment. We assume that the magnitude of the convolution effect is identical for vacancy and for adatom clusters, i.e. $\Delta N^{vac} = \Delta N^{ad} = \Delta N$. For completeness, we note that ΔN must not be an integer number.

Fig. 4 shows the result obtained after applying this approach for the apparent sputtering yield Y^* as a function of temperature for various values of ΔN, with $\Delta N = 0$, 0.25, 0.3, 0.35, 0.5 in units of linear atom size. Here, the evaluation of the integrated areas has been made using the average cluster size for each given temperature. Taking the full size distributions into account will not yield sizable deviations. The result for $\Delta N = 0$ is replotted from the inset of Fig. 2 and it is obviously non-physical. The result for $\Delta N = 0.5$ leads to a strong decrease of the apparent sputter yield from about 1.6 at 200 K to 0.7 at 350 K. This latter result is in contradiction with our assumption which requires a temperature independent apparent sputter yield. Based on our previous assumptions, the apparent sputter yield is best approximated for $\Delta N = 0.3$ which is reasonable in all respects. Another encouraging fact is that the deconvolution leads to quite minor changes for the data obtained at 350 K. The apparent sputter yield at this temperature is 0.7 copper atoms per incident ion. The excursion of the data at 275 K is attributed to a slightly deviating shape of the STM tip. However, the overall picture appears quite reasonable.

The integrated areas of adatom and vacancy clusters, after eliminating the errors due to convolution effects with a $\Delta N = 0.3$, are shown in Fig. 5. The solid lines guide the eye for the temperature dependence of the integrated area of the two species. The overall trend of the data in Fig. 5 is much improved compared to the previously shown data in Fig. 2, i.e. before the convolution effects exclusion. An exception is observed at 275 K where the adatom coverage is still higher than the vacancy coverage. We attribute this effect to a slightly deviating tip shape, i.e. less sharp STM tip.

The reduction of the integrated areas in the 225 K–300 K temperature regime and the plateau at higher temperatures in Fig. 5 is ascribed to the site selective interlayer mass transport taking place on the eroded Cu(001) surface. The annihilation of an adatom cluster with an existing vacancy island is favored by a facile descent of an adatom via a kink site which are quite abundant in the low temperature regime on the ion eroded Cu(001) surface. An atom attempting to descent a step edge needs to overcome an additional energetic barrier E_{ES} which is commonly referred to as *Ehrlich–Schwoebel barrier* [24,25]. It is this latter additional barrier that plays a key role in the enhanced interlayer mass transport in the 225 K–300 K temperature range in Fig. 5. An atom descending a step edge via a kink site experiences a negative E_{ES} barrier of − 5 meV [26]. In our experiments, in the low temperature regime, the vacancy islands have relatively small sizes, thus there is a large areal density of kinks. An adatom residing in the close vicinity of a small vacancy island will therefore easily find its way down via a kinked site. Although one would expect an increase in annihilation processes with a further increase of surface temperature, our experiments suggest that in the 300 K–325 K temperature range, the interlayer mass transport is inhibited. The plateau at these temperatures in Fig. 5 can be rationalized as follows. For sputtering at elevated substrate temperature, due to the effective surface diffusivity, large vacancy islands are formed. They will easily assume their equilibrium shape: square islands with steps oriented along the densely (close) packed ⟨110⟩ direction [29,30]. In this situation, an adatom will experience much higher barriers in its attempts to descend the ⟨110⟩ oriented step edge because of a much lower density of kinks per unit step length. The increase in vacancy island size with temperature will further diminish the descend probability of an adatom since it can not easily find kinks that could provide a channel for its descent. Note that the descent across a ⟨110⟩ segment is associated with a much higher ES barrier of > 120 meV. In literature, broad agreement has been reached about the fact that a descent across a ⟨110⟩ step requires substantially higher thermal activation than a descent across a ⟨110⟩ step, although the actual values for the barriers deviate considerably [27,28]. This difference in mass transport across ⟨110⟩ and ⟨110⟩ oriented step edges was in fact responsible for the observed pit rotation in ion sputtering experiments performed by Broekman et al [31]. In their study, the transition from a ⟨110⟩ oriented pits to a ⟨110⟩ pits is observed to take place at 275 K. This latter piece of information agrees with our experimental findings related to the plateau at 300 K–325 K in Fig. 5. At 350 K the interlayer mass transport is very effective, which results in a decrease of both the adatom and vacancy island integrated surface areas. However, the reduction in adatom covered surface fraction is not identical to the fraction of annihilated vacancies. Although we assumed that migration of bulk defects is ruled out in this temperature regime, at 350 K we are not far from its onset [21].

Although the systematic errors introduced by the STM tip (i.e. convolution effects) in our sputter yield determination have been eliminated, the value of the sputter yield inferred from our STM measurements (0.7 atoms/ion and equal to the apparent sputter yield) is still smaller than the value previously determined using the weight loss method. This seems reasonable since, in the temperature regime discussed here, the bulk vacancies do not contribute to the sputter yield. To get a better estimate of the sputter yield, we need to incorporate the latter in our analysis. For this purpose, we attempt to give an estimate of the number of bulk vacancies. A maximum estimate for the number of the bulk vacancies can be derived if one considers that surface vacancies are created by atoms expelled to the vacuum. Surface adatoms are than solely created by interstitials that have ascended to the surface.

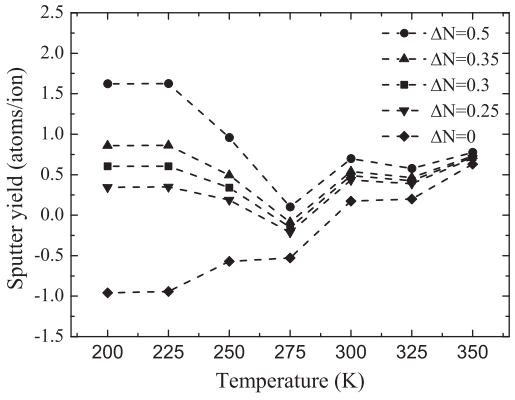

Fig. 4. The temperature dependence of the apparent sputter yield for various values of ΔN.

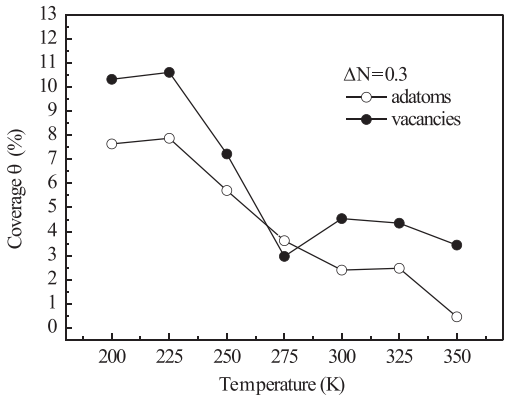

Fig. 5. Recalculated integrated areas for adatom (open circles) and vacancy (filled circles) clusters after deconvolution with $\Delta N = 0.3$. The solid lines connecting the experimental data guide the eye for the temperature dependence of the integrated areas. The anomalous behavior at 275 K is ascribed to a change in tip shape.

The creation of each interstitial is accompanied by the creation of a bulk vacancy. Therefore each interstitial that has not recombined with a bulk vacancy is identified as a surface adatom and is in this limit equivalent to the amount of hidden bulk vacancies, i.e. $\theta^{ad} = \theta^{bv}$ and the sputter yield reduces to: ($Y = \theta^{sv}\theta^{ion}$) Fig. 5 shows that at 200 K the coverage of surface vacancies is a little over 10%, leading to an upper limit of the sputter yield of 2.3 atoms/ion.

An even more realistic estimation of the sputter yield takes into account the atoms ejected from surface positions as well, which have a finite probability of being trapped by the surface potential and thereby transforming in adatoms. In this case, adatoms are created very close to surface vacancies and have a high probability to recombine with the latter when thermally activated [32]. This gives rise to the measured decay of adatom coverage in the 225 K–300 K temperature range in Fig. 5. On the other hand, one should expect that adatoms resulting from interstitials created at deeper positions show a lower positional correlation with surface vacancies and therefore a lower probability for annihilation. If we ascribe the observed plateau at 300 K–325 K to this effect, we can establish the number of adatoms issued from direct surface ejection and the amount of adatoms due to interstitial migration. In this case, the total observed adatom coverage (7.7%) at 200 K incorporates the adatoms originating from the surface layer (5.3%) and the remaining 2.4% originating from interstitial migration. With these last pieces of information, together with the available numbers for coverages at 200 K and with the assumption that the coverage of adatoms resulting from interstitials migration are indicative for the amount of bulk vacancies, we determine a more realistic value of the sputter yield of 1.2 copper atoms/ion. Further confidence in the correctness of this result is obtained from a comparison with Ref. [16]. For various conditions it was claimed that the number of adatoms per incident ion scales with the sputter yield by a factor of two. If we apply the same procedure we find for the number of adatoms per incident ion 0.105/0.044 = 2.39. Halving that number would lead to a sputter yield of 1.2 in excellent agreement with the value mentioned above.

Finally we would like to address one last issue that could give rise to a dissimilar sputter yield between weight loss measurements and STM. An essential difference between the present STM study and the previously mentioned sputter yield determination is the magnitude of the ion erosion given to the target. In our STM study the target was subjected to a mild erosion on an atomically flat Cu(001) surface, whereas in weight loss methods the target is subjected to extended sputtering. Upon extended ion erosion, the surface roughness that develops during sputtering can alter the energy deposited by the ion. A local variation in energy deposition on a roughened surface according to Sigmund's theory [33] was used by Bradley and Harper as one of the driving forces to explain pattern formation during ion sputtering [34]. Studies reported differences in sputter yields of 10% to 25% for flat and roughened surfaces, respectively [19,35]. Consequently, the sputter yield would have a tendency to increase with ion fluence. This is further corroborated by the substantial variation of the sputter yield with dose as calculated by Makeev and Barabási [36].

5. Conclusions

In this paper, we have reported a STM investigation of the sputter yield of a pristine Cu(001) surface after mild Ar^+ ion erosion. From a comparison of integrated areas of adatoms and surface vacancies, we infer an apparent sputter yield of about 0.7 copper atoms per 800 eV Ar^+ ion at normal incidence. This value provides a lower limit for the sputter yield due to the limited mobility of bulk vacancies in the temperature regime accessible in our measurements. An upper limit of the sputter yield is obtained by assuming that all adatoms result from interstitials arriving at the surface. The maximum value for the sputter yield is then 2.3 atoms/ion. This determines a range that covers the values measured previously using the weight loss method. We suggest that a more likely value for the total sputtering yield is 1.2 atoms/800 eV Ar^+ ion, which is derived by considering the quite high positional correlation between ion impacts and adatoms.

References

[1] J.G.C. Labanda, S.A. Barnett, L. Hultman, J. Vac. Sci. Technol., B 16 (4) (1998) 1885.
[2] A. Benninghoven, Phys. Status Solidi (a) 34 (1969) K169.
[3] M. Ritter, M. Stindtmann, M. Farle, K. Baberschke, Surf. Sci. 348 (1996) 243.
[4] S. van Dijken, D. de Bruin, B. Poelsema, Phys. Rev. Lett. 86 (2001) 4608.
[5] H. Hansen, A. Redinger, S. Messlinger, G. Stoian, Y. Rosandi, H.M. Urbassek, U. Linke, T. Michely, Phys. Rev. B 73 (23) (2006) 235414.
[6] U. Valbusa, C. Boragno, F. Buatier de Mongeot, J. Phys. 14 (2002) 8153.
[7] R. Behrisch, J. Bohdansky, G.H. Oetjen, J. Roth, G. Schilling, H. Verbeek, J. Nucl. Mater. 60 (1976) 321.
[8] N. Laegreid, G.K. Wehner, J. Appl. Phys. 32 (1961) 365.
[9] A. Oliva-Florio, R.A. Baragiola, M.M. Jakas, E.V. Alonso, J. Ferrón, Phys. Rev. B 35 (5) (1987) 2198.
[10] B. Poelsema, L.K. Verheij, G. Comsa, Phys. Rev. Lett. 53 (1984) 2500.
[11] B. Poelsema, R. Kunkel, L.K. Verheij, G. Comsa, Phys. Rev. B 41 (1990) 11609.
[12] H. Hansen, C. Polop, T. Michely, Phys. Rev. Lett. 92 (2004) 246106.
[13] G. Costantini, F. Buatier de Mongeot, C. Boragno, U. Valbusa, Phys. Rev. Lett. 86 (2001) 838.
[14] C. Teichert, M. Hohage, T. Michely, G. Comsa, Phys. Rev. Lett. 72 (1994) 1682.
[15] H. Gades, H.M. Urbassek, Phys. Rev. B 50 (1994) 11167.
[16] T. Michely, C. Teichert, Phys. Rev. B 50 (15) (1994) 11156.
[17] A.A. Promokhov, V.A. Eltekov, V. Yurasova, J. Colligon, A. Mosunov, Nucl. Instrum. Methods B 115 (1996) 544.
[18] T.W. Snouse, L.C. Haughney, J. Appl. Phys. 37 (1966) 700.
[19] A.L. Southern, W.R. Willis, M.T. Robinson, J. Appl. Phys. 34 (1963) 153.
[20] W. Ehrhardt, Atomic defects in metals, Vol. 25 of Landolt-Börnstein, Springer-Verlag, 1991.
[21] H.G. Bowden, R.W. Balluffi, Philos. Mag. 19 (1969) 1001.
[22] J.M. Fluit, C. Snoek, J. Kistemaker, Physica 30 (1964) 144.
[23] R.S. Nelson, Philos. Mag. 11 (1965) 291.
[24] G. Ehrlich, F.G. Hudda, J. Chem. Phys. 44 (1966) 1039.
[25] R.L. Schwoebel, J. Appl. Phys. 40 (1969) 614.
[26] F. Rabbering, H. Wormeester, F. Everts, B. Poelsema, Phys. Rev. B 79 (2009) 075402.
[27] M. Li, J.F. Wendelken, B.G. Liu, E.G. Wang, Z. Zhang, Phys. Rev. Lett. 86 (11) (2001) 2345.
[28] O.S. Trushin, K. Kokko, P.T. Salo, W. Hergert, M. Kotrla, Phys. Rev. B 56 (19) (1997) 12135.
[29] G. Costantini, S. Rusponi, F. Buatier De Mongeot, C. Boragno, U. Valbusa, Surf. Sci. 416 (1998) 245.
[30] Ch. Teichert, Ch. Ammer, M. Klaua, Phys. Status Solidi A 146 (1994) 223.
[31] P. Broekmann, A. Mewe, H. Wormeester, B. Poelsema, Phys. Rev. Lett. 89 (14) (2002) 146102.
[32] M. Morgenstern, T. Michely, G. Comsa, Philos. Mag. A 79 (1999) 775.
[33] P. Sigmund, Phys. Rev. 184 (1969) 383.
[34] R.M. Bradley, J.M.E. Harper, J. Vac. Sci. Technol. A6 (1988) 2390.
[35] D. Onderdelinden, Ph.D. thesis, University of Leiden (1968).
[36] M.A. Makeev, A.-L. Barabási, Appl. Phys. Lett. 73 (1998) 1445.